

# Passive optical detection of submillimeter and millimeter size space debris in low Earth orbit



Mike Gruntman\*

Department of Astronautical Engineering, University of Southern California, Los Angeles, CA 90089-1192, USA

## ARTICLE INFO

### Article history:

Received 4 March 2014

Received in revised form

6 August 2014

Accepted 21 August 2014

Available online 30 August 2014

### Keywords:

Space debris

Passive optical debris detection

Photon-counting detector

Proximity sensing

Space situational awareness

Mission assurance

## ABSTRACT

Understanding of the space debris environment and accuracy of its observation-validated models are essential for optimal design and safe operation of satellite systems. Existing ground-based optical telescopes and radars are not capable of observing debris smaller than several millimeters in size. A new experimental and instrumental approach – the space-based Local Orbital Debris Environment (LODE) detector – aims at in situ measuring of debris with sizes from 0.2–10 mm near the satellite orbit. The LODE concept relies on a passive optical photon-counting time-tagging imaging system detecting solar photons (in the visible spectral range) reflected by debris crossing the sensor field of view. In contrast, prior feasibility studies of space-based optical sensors considered frame detectors in the focal plane. The article describes the new experimental concept, discusses top-level system parameters and design tradeoffs, outlines an approach to identifying and extracting rare debris detection events from the background, and presents an example of performance characteristics of a LODE sensor with a 6-cm diameter aperture. The article concludes with a discussion of possible sensor applications on satellites.

© 2014 IAA. Published by Elsevier Ltd. All rights reserved.

## 1. Submillimeter and millimeter debris in low-Earth orbit

Artificial satellites, rocket bodies, and their fragments orbit the Earth in increasing numbers and present danger to operational spacecraft, especially in low-Earth orbit (LEO) and geostationary orbit (e.g., [1–7]). The United States and the former Soviet Union, now Russia, have been operating a combination of radar and optical means for cataloging and monitoring space objects since 1960s [3,7–9]. Other countries in Asia and Europe, particularly the People's Republic of China and the European Space Agency (as well as national programs in France and Germany), strive to expand their capabilities in the space situational awareness.

The knowledge of the deteriorating space debris environment and accuracy of its observation-validated models are essential for optimal design and safe operation of satellite systems. The U.S. Space Surveillance Network routinely detects, tracks, and catalogs more than 16,000 orbiting space objects larger than 5–10 cm in LEO, with 400,000 observations taken each day [10]. Much more numerous debris smaller than several centimeters also orbit the Earth. Estimates put the number of debris with sizes from 1 mm to 10 cm in tens of millions and smaller than 1 mm in trillions [3]. Properties of such objects are characterized statistically rather than individually.

A collision with a large, > 5 cm, object would likely cause a loss of a spacecraft and its catastrophic breakup [3], creating numerous fragments. Just one anti-satellite weapon test by the People's Republic of China in January 2007 [11] contributed more than 150 thousand debris one centimeter and larger in LEO [12]. Large orbiting objects are individually observed and cataloged and accidental

\* Tel.: +1 213 7405536.

E-mail address: [mikeg@usc.edu](mailto:mikeg@usc.edu)

collisions with them can thus be sometimes avoided. Populations of very small debris, <0.1 mm, can be experimentally studied and statistically characterized by bringing exposed surfaces back to Earth from orbit (e.g., LDEF, SMM, EURECA, SFU, and Space Shuttle) and examining collision effects [7]. These very small debris could cause degradation of surfaces and perhaps damage unprotected spacecraft components.

This work concentrates on the population of debris with intermediate sizes from 0.1–10 mm. Such submillimeter (0.1–1 mm) and millimeter (1–10 mm) debris are typically too small to be detected by existing optical and radar means, and there are too few of them to be described by studying exposed surfaces. Because of this gap in observations [7,13,14], one has to rely on modeling of their populations based on difficult to accurately predict processes in breakup of complex bodies in high-velocity impacts. At the same time possible damage to spacecraft by submillimeter and millimeter debris ranges from surface degradation to possible loss of spacecraft capability or its components [3].

Atmospheric drag lowers orbital altitudes of space objects in LEO and causes their eventual reentry into the atmosphere. (Solar radiation pressure may also become important for some objects with large area-to-mass ratios.) Drag acceleration acting on an orbiting body is inversely proportional to its characteristic size. Consequently, the acceleration becomes higher and the lifetime in the orbit shorter with the decreasing size of the body. For example, drag would remove an aluminum sphere 1-mm in diameter from an initial 400-km altitude orbit within a couple of weeks. Such altitudes are especially important for human spaceflight (International Space Station) and atmospheric drag effectively reduces danger of small debris in such orbits.

At higher altitudes from 700–1500 km with numerous application satellites, lifetimes of orbiting objects may exceed dozens or hundreds of years, resulting in accumulation of debris. Existing ground-based optical and radar systems have inherent limitations in measuring dangerous to satellites submillimeter and millimeter debris at these altitudes.

First, only ground-based systems near the equator can probe space objects in low-inclination low-Earth orbits, limiting capabilities of facilities in the continental United States. In addition, ground optical systems can observe LEO objects only during short time intervals at local dawn and dusk.

Second, for radar, the efficiency of electromagnetic radiation scattering, characterized by radar cross-sections, rapidly decreases for small objects, e.g., [15]. For example, the radar cross-section of a perfectly conducting sphere with a diameter at least three times larger than the wavelength approximately equals its geometric cross-section. For spheres with diameters less than one-third of the wavelength, radar cross-sections drop precipitously (known as Rayleigh scattering) with decreasing diameters.

Most existing and planned (such as the upgrade of the Space Fence in the United States) radars operate in the S-band frequencies with wavelengths 6–15 cm. For example, a perfectly conducting 1-mm diameter sphere would

have the radar cross-section almost 5 orders of magnitude smaller than its geometric cross-section for a typical S-band radar operating at the 3 GHz frequency (wavelength 10 cm). For an X-band radar at the 10 GHz frequency (wavelength 3 cm), the corresponding radar cross-section would be 800 times smaller. Atmospheric absorption (e.g., [16]) fundamentally limits possible increase of radar frequencies beyond the X-band required for further lowering the upper size limit of the Rayleigh scattering region.

The German Fraunhofer Institute's Tracking and Imaging Radar (TIRA) near Bonn operating autonomously or in a bistatic mode (with the Max-Planck-Society's radio telescope at Effelsberg) could detect orbiting debris as small as 1–2 cm at altitudes up to 1000 km [5]. Most capable NASA radars today, the Haystack and Goldstone, can detect debris down to several millimeters in size at important for human spaceflight 400-km altitudes [7,17]. In recent years, the upgraded Haystack and Haystack Auxiliary (HAX) radars also demonstrated detection of such debris at 800 km altitude [18] where numerous satellites operate and where debris accumulate due to significantly diminished atmospheric drag.

Satellite-based (space-based) optical sensors offer important opportunities especially for detecting large orbiting objects as was demonstrated, for example, by the Space-Based-Visible sensor on the Midcourse Space Experiment, or MSX [19,20]. A number of feasibility studies examined capabilities of possible space-based passive optical sensors for measuring millimeter and/or centimeter size debris and larger in LEO [13,14,21–23] as well as observing objects in geostationary orbit [13,14,21,22,24,25]. (For the sake of completeness, we also note here an assessment of a space-based radar for detecting objects in LEO [26].) To the best of my knowledge no study has specifically looked at optical observation of submillimeter debris.

At the same time, a recent NASA Handbook [7] especially emphasizes the importance of such submillimeter debris by stating that “from the safety and satellite operations perspective, there is an immediate need for a large and dedicated meteoroid and orbital debris sensor to monitor and update the populations between 0.1 and 1.0 mm.” A special feasibility study sponsored by the European Space Agency specifically focused on closing “the existing knowledge gap in the space debris population in the millimeter and centimeter regime” [14]. Scarcity of experimental data leads to a one-order-of-magnitude disagreement among debris models (ORDEM, MASTER, SDPA) in prediction of fluxes of debris smaller than 1 cm [7].

This article describes a new space-based experimental and instrumental concept – the Local Orbital Debris Environment (LODE) detector – to observationally characterize 0.2–10 mm debris near the satellite path important for space system design and for mission assurance and safe operation. It concentrates on top-level system parameters and design tradeoffs, outlines an approach to identifying and extracting rare debris detection events from the background, and presents an example of performance characteristics of a LODE sensor with a 6-cm diameter aperture. Specific designs of the optical part of

the sensor and its focal plane detector are beyond the scope of the article. While the LODE concept primarily focuses on observation of debris in LEO, it can also probe micrometeoroid fluxes, debris at geostationary orbit, and perhaps dust in the lunar environment.

## 2. LODE sensor concept

The Local Orbital Debris Environment sensor is based on a passive optical photon-counting time-tagging imaging system deployed on a spacecraft and detecting solar photons (in the visible range) reflected by debris crossing its field of view (Fig. 1). The sensor would thus characterize the debris population locally within a certain distance from the satellite orbit path. Sensor pointing in a general antisolar direction on a spacecraft in dawn–dusk (equator crossing) sun-synchronous orbit offers most favorable observation geometry in LEO. The instrument could fly on a dedicated small satellite or as a hosted payload.

Prior flown or studied space-based optical sensors for debris detection used CCD (charged-coupled device) detectors in the focal plane [13,14,19–22,24,25]. The CCDs are essentially frame detectors. A passage of an object across the field of view during the frame accumulation time interval results in an image of a streak across a pattern of fixed stars and diffuse background. Arrival of 20 or more photons into the instrument is usually needed for a signal above the intrinsic noise in a single CCD pixel. Reliable detection of a rare debris streak requires a sequence of multiple lighten-up pixels and correspondingly at least a few hundred debris-reflected photons.

The LODE concept differs from considered in the past approaches by relying on a different type of focal-plane detectors that enable the desired capabilities. Specifically, the resulting reduced number of photons needed for detection of an object crossing the sensor field of view (FOV) opens a way for observing smaller submillimeter and millimeter debris. To the best of my knowledge, in

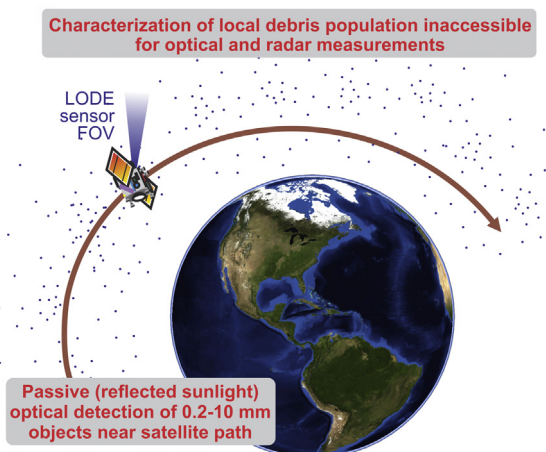
addition to purely astronomical applications, e.g., [27–30], such space- and ground-based visible-range photon-counting time-tagging imaging systems were considered in the past only for imaging of complex three-dimensional objects (such as satellites) and non-local (i.e., at large distances) detection of centimeter size debris [23,31,32]. Nobody considered applications of such systems for detection of submillimeter and millimeter debris locally near the satellite path.

The LODE instrument relies on a microchannel-plate (MCP) based position-sensitive detector (PSD) in the focal plane. Such detectors have been used in laboratory and space applications registering and determining coordinates of individual particles and photons since 1970s (see, e.g., reviews [33–39] and references therein). For example, two currently operating Hubble Space Telescope instruments include detectors of this type [29,30]. While MCP-based detectors are less common in satellite-based astronomical and astrophysical instruments, they are routinely used (though without photocathodes), in space physics experiments. Consequently, the associated technology readiness levels of MCP detectors, readout electronics, and high voltage (usually not exceeding 2–3 kV) power supplies are very high.

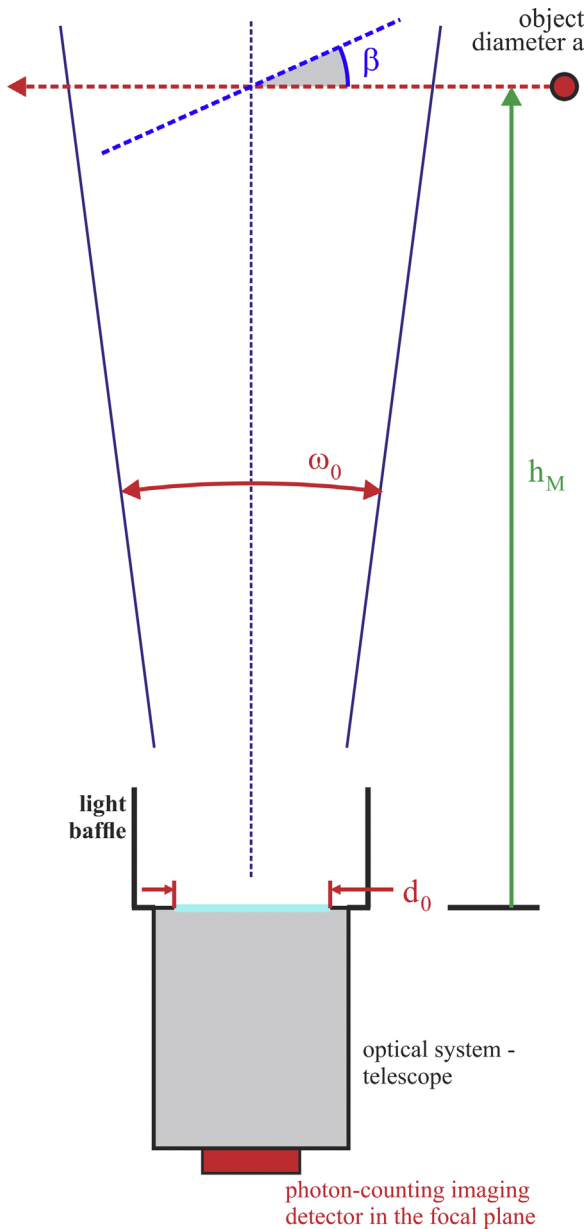
Such photon-counting imagers are fundamentally different from CCD-based systems. In contrast to CCDs, an MCP-based PSD does not accumulate a frame image but determines in real time the coordinates (in the focal plane) and the exact detection time of each registered individual photon and stores them in a memory. A computer can then use such data in asynchronous post-processing to form an image accumulated during any desired time interval while preserving timing information, or time tags, of each and all registered photons. These unique capabilities of photon-counting time-tagging imagers enable the proposed concept.

Fig. 2 shows the schematic of a LODE imager. It consists of an optical system, a simple telescope, with the entrance aperture diameter  $d_0$  and field of view angle  $\omega_0$  and a photon-counting imager at the focal plane. A baffle reduces light from off-axis bright sources such as the Moon and atmospheric glow. Due to spacecraft orbital motion, the relative velocity of debris would be predominantly in the direction opposite to the spacecraft velocity vector. Therefore, pointing the LODE sensor normally to the orbital plane would maximize the number of crossings of the instrument FOV by debris.

When a FOV crossing occurs, registered photons would form a well-determined sequence, or line (a “trajectory”), in three-dimensional  $(x, y, t)$  “sensor space” of two spatial coordinates-directions  $x$  and  $y$  in the detector focal plane (similarly to a streak captured by CCD detectors) and additionally in the dimension of time. In contrast, background photons would form a random pattern of counts in spatial and time dimensions. Registration of only several debris-reflected photons is sufficient to reliably identify an object FOV crossing. Therefore, arrival of a relatively small number, only a few dozen, of photons into the LODE sensor with a realistic photon detection efficiency is needed. Consequently, this sensitive technique offers observational access to submillimeter and millimeter debris inaccessible to conventional radar and optical means. The observation



**Fig. 1.** Local Orbital Debris Environment (LODE) concept for in situ characterization of debris population in the 0.2–10 mm size range near the satellite orbit by passive optical detection of debris-reflected solar photons in the visible spectral range. FOV – the field of view of the sensor.



**Fig. 2.** Schematic of the LODE sensor: optical telescope with the aperture diameter  $d_0$  and field of view  $\omega_0$  and a photon-counting time-tagging imaging detector in the focal plane. An object of a diameter  $a$  crosses normally the field of view at the maximum detection distance  $h_M$ ; also shown is a trajectory crossing the instrument axis at an angle  $\beta$ .

of a FOV crossing event would constrain in an important way a combination of parameters characterizing this particular debris trajectory, size, albedo, and velocity.

The count rate limitations of MCP-based PSDs results, as shown below in Section 3, in a relatively narrow field of view of the LODE sensor, a small fraction of one degree. In contrast, passive CCD-based optical sensors usually relied on relatively wide fields of view. For example, the MSX's Space-Based Visible sensor had a 15-cm aperture telescope with the  $1.4^\circ \times 6.6^\circ$  field of view [19,20] while other considered systems had, for example, 7.5-cm aperture

and  $20^\circ$  FOV [21]; 10-cm aperture and  $1^\circ$  FOV [13]; and 20-cm aperture and  $6^\circ$  FOV [22]. The LODE imager could thus be, in an important sense, complementary to CCD-based optical sensors and perhaps they could be combined in a package offering unique cross-calibration and debris-characterizing capabilities.

### 3. LODE sensor performance characteristics

A photon-counting imaging detector (Fig. 3) consists of a photocathode followed by a stack of MCPs and an electron collector-anode with its readout circuitry determining the coordinates of each registered incident photon [33–39]. For visible spectral range, the photocathode is usually deposited on the back side of a transparent entrance window, with photoelectrons accelerated across a small gap (so-called proximity focusing) in a compact design towards the entrance of the MCP. The MCP stack of two or three plates converts the photoelectron into an avalanche of  $10^6$ – $10^8$  electrons falling on the anode. A sealed vacuum tube confines the photocathode side of the window, the MCP stack and the collector-anode (Fig. 3). The electronic circuitry determining photon coordinates and detection moments of time as well as the high-voltage (2–3 kV) power supply are outside the sealed tube.

A number of readout designs have been developed for PSDs based on charge division, multianode discrete elements, and delay lines [33–45]. Various approaches are particularly suitable for different applications and the design can be optimized to achieve specific LODE requirements. The PSD sensitive area can vary from 15–100 mm with spatial resolution up to 2000 pixels in each dimension. The detectors can also determine the moment of photon detection with accuracy as high as a fraction of 1 ns (e.g., [46,47]). The LODE sensor requires, as discussed below, much more modest spatial resolution and timing accuracy of the PSD.

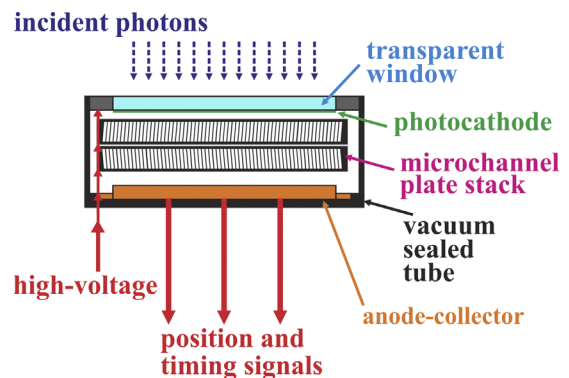


**Fig. 3.** Schematic of a microchannel-plate position-sensitive detector. Such photon-counting time-tagging imaging detectors determine in real time the coordinates and moment of time of detection of each registered incident photon. The detector consists of a transparent window with the photocathode, microchannel plate stack, and anode-collector in a vacuum-sealed tube with connectors for high voltage power and for signal output. A photoelectron produced by an incident photon from the photocathode is accelerated toward the MCP stack that converts it into an avalanche of  $10^6$ – $10^8$  electrons falling on the readout anode-collector.

Diffuse background light intensity and individual bright stars constrain the LODE aperture area and the field of view. The maximum total count rate,  $C_M$ , of MCP-based detectors is usually limited to  $10^5$ – $10^6$   $s^{-1}$  for fluxes distributed uniformly across the sensitive area. For point star-like sources, the count rate could be limited to only 10–100  $s^{-1}$ , depending on a particular design of the MCP stack. The MCP gain substantially decreases locally for intensities above that point-source maximum count rate limit.

Zodiacal light, integrated starlight of unresolved stars, and diffuse galactic light dominate the background light intensity for an observer above the atmosphere [48]. The color of the zodiacal light is close to that of the solar light; this work also assumes the spectral distribution of starlight to be similar to that of the Sun. Different units are used to describe background light intensity (phot  $cm^{-2} s^{-1} sr^{-1}$ ) or brightness (see [48] for relations among various units). Some publications use units  $S10_s$  which correspond to brightness of one solar type star of tenth magnitude per degree squared. Other publications often describe brightness in other similar units  $S10$  which is brightness of one A0 type star of tenth magnitude per degree squared. These units are close to each other with differences dependent on specific spectral range. In addition, intensities produced by a star of a certain apparent magnitude in a field of view of one square arcsecond are also used.

Zodiacal light brightness depends on ecliptic latitude and peaks in the ecliptic plane. It also strongly depends on viewing direction with intensity rapidly rising with approach to the Sun. In antisolar directions, zodiacal light brightness does not exceed 200  $S10$  [48].

Brightness of the galactic background that includes stars dimmer than apparent magnitude 6.5 varies from less than 50  $S10_s$  near galactic poles to 500–600  $S10_s$  near the galactic equator [48,49]. (Diffuse galactic light constitutes about 20–30% of the total galactic background.) A satellite sensor pointed in an antisolar direction would thus be exposed to galactic brightness above 200  $S10_s$  only during a small fraction of the year when its FOV crosses the galactic plane. Brightness of extragalactic background does not exceed 20  $S10_s$  [49].

For conservative estimates, this work assumes the total background light intensity to be 500  $S10_s$ . Prior studies of space-based sensors used either similar background corresponding to one star of 21 magnitude per square arcsecond, or  $m_V = 21$  mag/arcsec<sup>2</sup>, [13,14] or lower intensities, such as  $m_V = 21.5$  mag/arcsec<sup>2</sup> [22] and  $m_V = 22$  mag/arcsec<sup>2</sup> [25], the latter value corresponding to 205  $S10$  [48]. High performing visible-light optimized S-20 photocathodes are mostly sensitive in the 450–850 nm spectral range, with the wavelength-dependent quantum efficiency varying from 7–16% [39,50]. The solar photon flux density is  $F_S = 2 \times 10^{17}$  phot  $cm^{-2} s^{-1}$  in this range at 1 AU. Consequently, the background light intensity  $f_0$  corresponding to 500  $S10_s$  in this spectral range would be

$$f_0 \approx 6.1 \times 10^8 \text{ phot cm}^{-2} \text{ s}^{-1} \text{ sr}^{-1} \approx 8300 R,$$

where 1  $R = 1$  Rayleigh =  $10^6 / (4\pi)$  phot  $cm^{-2} s^{-1} sr^{-1}$ . Consider now a photon-counting imaging sensor (Fig. 2)

with the aperture diameter  $d_0$ , field of view solid angle  $\Omega_0$ , and photon detection efficiency  $\varepsilon_0$ . The maximum possible count rate of the detector,  $C_M$ , constrains the sensor geometric factor,  $\Omega_0 \sigma_0$ , as

$$C_M = f_0 \varepsilon_0 \Omega_0 \sigma_0, \quad (1)$$

where  $\sigma_0 = \pi d_0^2 / 4$  is the aperture area. The sensor FOV plane angle width is

$$\omega_0 = \sqrt{\frac{4\Omega_0}{\pi}} = \frac{4}{\pi d_0} \left( \frac{C_M}{f_0 \varepsilon_0} \right)^{1/2}. \quad (2)$$

A large solid angle could result in a high probability of a sufficiently bright star appearing in the imaged region of the sky, affecting the detector performance. Bright stars could thus make a portion of the sky inaccessible for sensor pointing. Fig. 4 shows the dependence of the photon count rate density (count rate per unit area of the sensitive surface) for a sensor with an S-20 type photocathode as a function of star apparent magnitudes under the assumption of the solar spectral distribution. Both the detector response to individual stars and the limit on the diffuse background maximum count rate  $C_M$  would determine apertures and fields of view of realistic LODE sensors. An MCP-based detector with an S-20 type photocathode usually exhibits an intrinsic (uniformly distributed across the sensitive surface) noise count rate density 5–20 count  $cm^{-2} s^{-1}$ . The MCP stack contributes only about 1 count  $cm^{-2} s^{-1}$  to these counts while most of the noise is produced by photoelectrons emitted from the photocathode. The LODE detector is protected from direct exposure to the near-Earth energetic particle environment. One could expect only modest increase, perhaps doubling, of its already small MCP intrinsic noise contribution largely due to cosmic rays, with the overall photocathode-determined noise count rate remaining practically unchanged. In any case, it is the diffuse light background that is responsible for a couple orders of magnitude larger numbers of detected photons which, in turn, are determined by the selected maximum count rate  $C_M$ . This background rather than the PSD noise would thus constrain the effective dynamic range

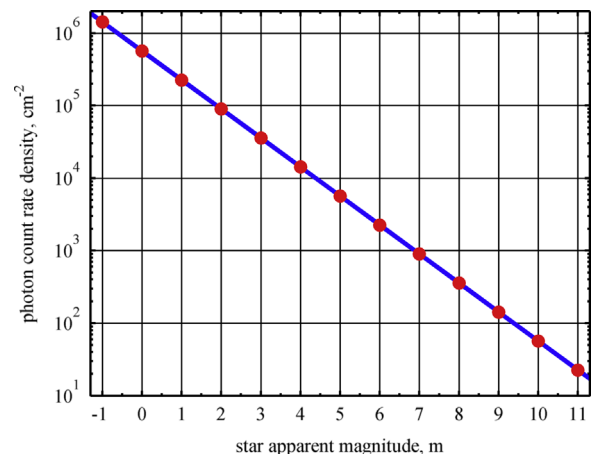


Fig. 4. Count rate density (per square centimeter per second) of a sensor sensitive area as a function of star apparent magnitude for assumed solar spectral distribution and quantum detection efficiency of the typical S-20 type photocathode.

of the detector. A required very modest spatial resolution of the LODE (perhaps as low as 128 pixels across the sensitive surface, as discussed in Section 4) also eliminates any contribution to the noise by the readout electronics. To summarize, the detector noise is much smaller than the count rate due to the expected diffuse photon background and can thus be disregarded.

Consider now an object (debris) with an effective illuminated diameter  $a$ , effective illuminated area  $A = \pi a^2/4$ , and effective albedo  $\alpha$  (reflection probability of photons in the spectral range of the detector sensitivity) at the distance  $h$  from the sensor. For a sensor pointed in the antisolar direction, the effective observed illuminated area of the object equals its area, and, for simplicity, there is no dependence on the illumination phase angle. To simplify the estimates, it is assumed that photons reflect isotropically into the  $2\pi$  hemisphere from a debris surface (this is somewhat different from perfectly diffuse, or lambertian, scattering).

The object-reflected solar photon flux density  $j_0$  at the LODE sensor and its corresponding photon count rate,  $C_0 = \varepsilon_0 j_0 \sigma_0$ , are

$$j_0 = \frac{F_S \alpha a^2}{8h^2}$$

and

$$C_0 = \frac{\pi F_S \alpha \varepsilon_0 d_0^2 a^2}{32 h^2},$$

respectively. The time  $\Delta t$  of crossing the narrow sensor field of view by an object with a relative velocity  $V_0$  perpendicular to the sensor axis (Fig. 2) is

$$\Delta t = \frac{\omega_0 h}{V_0} = \frac{4h}{\pi d_0 V_0} \left( \frac{C_M}{f_0 \varepsilon_0} \right)^{1/2}. \quad (3)$$

The average number  $N$  of object-reflected photons registered by the sensor during the FOV crossing would be

$$N = C_0 \Delta t$$

or

$$N = \frac{F_S \alpha}{8 V_0} \left( \frac{\varepsilon_0 C_M}{f_0} \right)^{1/2} d_0 a^2 = \frac{\pi^{1/2} F_S \alpha \varepsilon_0 \Omega_0^{1/2} d_0^2 a^2}{16 V_0 h}. \quad (4)$$

The last expression and a few other below are shown, for convenience, as functions of both (i)  $d_0$  and  $C_M$  and (ii)  $d_0$  and  $\Omega_0$ . One can see that the average number of registered photons depends on the product of the effective solar flux, detector efficiency, and albedo. This product is a simplified convolution of the solar flux spectral density distribution with the wavelength-dependent detection efficiency and albedo.

Let us require to register a certain minimum number  $M$  of object-reflected photons in order to reliably detect its FOV crossing. One can then introduce a maximum distance  $h_M$  (Fig. 2) at which a passing of an object with a diameter  $a$  results in registration, on average, of  $M$  photons,

$$h_M = \frac{1}{M} \frac{F_S \alpha}{8 V_0} \left( \frac{\varepsilon_0 C_M}{f_0} \right)^{1/2} d_0 a^2 = \frac{1}{M} \frac{F_S \alpha \varepsilon_0 \pi^{1/2} \Omega_0^{1/2}}{16 V_0} d_0^2 a^2. \quad (5)$$

A passage of an object larger in size and/or closer to the sensor would result in a larger average number of registered photons and consequent event detection.

The time interval  $\Delta t_M$  that it takes for an object to cross the field of view at the maximum detection distance  $h_M$  is

$$\Delta t_M = \frac{1}{2\pi M} \frac{F_S \alpha C_M a^2}{V_0^2 f_0} = \frac{1}{8} \frac{F_S \alpha \varepsilon_0}{M V_0^2} \Omega_0 d_0^2 a^2. \quad (6)$$

For given sensor properties, this time interval depends only on the object size and velocity. The average number of background photons  $N_B$  registered during  $\Delta t_M$  is

$$N_B = C_M \Delta t_M$$

or

$$N_B = \frac{1}{2\pi M} \frac{F_S \alpha C_M^2 a^2}{V_0^2 f_0} = \frac{\pi}{32} \frac{F_S \alpha f_0 \varepsilon_0^2 \Omega_0^2}{M V_0^2} d_0^4 a^2.$$

Let us introduce now the effective detection area  $S(a)$  of the LODE system for objects of a given size. If an object passes through this area then the event would be detected. For debris in circular orbits with uniformly distributed inclinations, the motion of the observer would cause most of the debris to move predominantly in the direction opposite to the velocity vector of the observer. Relative velocities of debris would vary from zero to twice the typical velocity of an object in low Earth orbit, the latter being 7.3–7.7 km s<sup>-1</sup>. To simplify the estimates, we assume henceforth the constant relative velocity  $V_0 = 10$  km s<sup>-1</sup> of passing objects pointed perpendicular to the LODE FOV direction (Fig. 2), the latter oriented normally to the spacecraft orbital plane. Such a relative velocity would be typical for debris crossing the spacecraft orbit perpendicularly.

Then, all the objects crossing the field of view cone at distances closer than the maximum detection distance would be detected. The effective detection area is the projected area of the FOV cone

$$S(a) = \frac{\omega_0 h_M^2}{2}$$

or

$$S(a) = \frac{1}{32\pi} \frac{F_S^2 \alpha^2 \varepsilon_0^{1/2}}{V_0^2} \left( \frac{C_M}{f_0} \right)^{3/2} \frac{d_0}{M^2} a^4 = \frac{\pi^{1/2} F_S^2 \alpha^2 \varepsilon_0^2 \Omega_0^{3/2} d_0^4 a^4}{256 V_0^2 M^2}. \quad (7)$$

The larger the effective detection area the more efficiently the LODE sensor detects debris passing by. The detection area steeply drops with the decreasing object size  $a$  which ultimately determines the lower limit of the debris size that could be observed. One can also see the importance of minimizing the required minimum number of debris-reflected photons  $M$  to be registered for object detection.

The introduced description of debris detection is essentially a threshold concept: debris of a given size are detected only when they cross the FOV at distances smaller than  $h_M$ . This oversimplified maximum detection distance concept, as discussed below, disregards the random nature of photon fluxes and their detection and the resulting statistical variations in the number of registered photons. Nevertheless, it is very useful in providing insight into the sensor performance and dependence of its characteristics  $h_M$ ,  $\Delta t_M$ ,  $N_B$ , and  $S$  on the debris size  $a$ .

We note here that some passing objects would not cross the sensor field of view center, resulting in fewer registered photons. For such objects, the maximum detection distance and effective detection area would correspondingly be smaller. This effect is disregarded in this work.

#### 4. LODE sensor example

Let us consider, as a realistic example, a LODE sensor with the aperture  $d_0 = 6$  cm in diameter. (Past concepts of space-based passive optical systems considered larger apertures: 7.5 cm and 40 cm [21], 15 cm [13,23], and 20-cm [14,22].) The LODE telescope would produce an image in the focal plane on the MCP-based PSD with a sensitive area 15–25 mm in diameter. We will make conservative estimates of the instrument properties, somewhat underestimating its performance characteristics.

Let us assume the maximum total detector count rate  $C_M = 10^4$  s<sup>-1</sup>. While MCP detectors could handle much higher rates up to  $10^6$  s<sup>-1</sup>, the assumed  $C_M$  would significantly simplify the processing of measurements, lower the required minimum number of registered debris-reflected photons  $M$ , and extend detector operations for years without deterioration of the photocathode efficiency and the MCP gain.

We assume the average PSD photon detection efficiency  $\varepsilon_0 = 0.10$  within the S-20 photocathode spectral sensitivity range of 450–850 nm. The efficiency of S-20 photocathodes is somewhat higher [39,50], so the adopted lower value here also accounts for photon losses in the optical part of the sensor. (Higher detection efficiencies could possibly be achieved in the future [23,38].)

The selected aperture diameter and the maximum count rate determine (Eqs. (1) and (2)) the solid angle  $\Omega_0 = 5.35 \times 10^{-6}$  sr and plane angle  $\omega_0 = 0.15^\circ$  of the sensor FOV. The diffraction limited resolution of the sensor is about  $0.00058^\circ$  which corresponds to 250 angular pixels across the field of view. Therefore, the spatial  $(x, y)$  resolution of the PSD need not be higher than  $250 \times 250$  pixels. As it is discussed below, a very modest resolution of 128 pixels across the detector sensitive area could suffice for debris detection. For a PSD 15–25 mm in diameter, the corresponding size of individual pixels would be 120–200 micron, or an order of magnitude larger than the size of MCP channels. Such a low spatial resolution provides flexibility in optimizing detector readout in an effective way.

An individual star with apparent magnitude  $m_V = 7.6$  would produce the assumed maximum count rate  $C_M$ . The MCP detector gain drops significantly for point star-type objects with much lower count rates  $10\text{--}100$  s<sup>-1</sup> [33–37] and it may get below the level of triggering the photon detection circuitry. For conservative estimates, we require avoidance of stars brighter than magnitude 7.6 in the field of view. There are about 25,000 such stars [51], and the avoidance requirement would thus exclude about 1.1% of the sky. Note that the background photon intensity of unresolved faint stars assumed in this work is based on the exclusion of stars brighter than magnitude 6.5 [49,50].

Therefore, the photon background with stars  $m_V = 7.6$  and brighter excluded would be somewhat smaller.

We assume the debris albedo  $\alpha = 0.15$ . The albedo of fragmented space debris is actually estimated to be as high as 0.175 [25,52], although the latter value was derived from observations of larger objects.

In order to estimate the desired minimum number  $M$  of registered debris-reflected photons for reliable identification of FOV crossings one needs to determine the probability that random background photons produce a pattern of registered photons indistinguishable from a true debris detection. It takes a certain time interval for an object with the assumed relative velocity to normally cross the sensor FOV at a selected distance (Eq. (3)). For example, it takes 1 ms to cross the FOV at the 3.8-km distance from the sensor. Therefore, one would consider photon counts registered during such a time interval for search of events of debris passage at that distance or closer.

Consider now searching for debris FOV crossing events during a time interval  $\Delta t$ . The average number of registered background counts would be  $k_B = C_M \Delta t$ . Let us assume the PSD spatial resolution to be  $n$  pixels in both  $x$  and  $y$  directions, with the total number of  $n^2$  pixels in the focal plane. The division of the time interval  $\Delta t$  into more than  $n$  time steps (bins) does not improve the accuracy because of the uncertainty introduced by the finite spatial pixel size. Therefore, we also assume  $n$  elements in the time dimension, with the time steps  $\delta t = \Delta t/n$ . (Note here that absolute step values  $\delta t$  depend on the chosen time interval  $\Delta t$ .)

Because of the narrow FOV of the LODE, the trajectories formed by passing debris in the sensor three-dimensional  $(x, y, t)$  space are straight lines. This means straight streaks in two-dimensional spatial images as well as linear time dependences of  $X$  and  $Y$  coordinates of registered photons. Possible exceptions would be only debris trajectories in directions close to the sensor axis at large angles  $\beta$  (Fig. 2), with correspondingly diminished detection areas. These low-probability events could be accounted for in detailed simulations of LODE properties which is outside the scope of this work.

There is a finite probability, however, that registered random background photons would also form a straight line in the sensor space, producing a “false” crossing event, and thus look indistinguishable from detection of a true debris. The straight line-trajectory in the  $(x, y)$  sensor plane has the length of  $n$  pixels and includes  $(1/n)$ -th of the total number of spatial pixels of the sensor. The average number of background photons detected in the pixels of that line is

$$k_0 = \frac{k_B}{n} = \frac{C_M \Delta t}{n}.$$

Consider now the first photon registered during the interval  $\Delta t$ . In order to register the required  $M$  background photons in the pixels of this particular line, one needs additional  $(M - 1)$  random background photons to be also detected on that line. The probability  $P_{M-1}$  of detection of these additional photons is then described by the Poissonian distribution and

$$P_{M-1}(k_0) = \frac{k_0^{M-1} \exp(-k_0)}{(M-1)!}.$$

The detection of the second photon during the time interval  $\Delta t$  with certain coordinates  $(x, y)$  and at a certain moment of time on the selected straight line determines the exact trajectory in the three-dimensional sensor space. Therefore, the following after that  $(M - 2)$  photons must be registered in precisely defined moments of time corresponding to their spatial coordinates in order to form the trajectory indistinguishable from the true passing object. The probability for a random photon to be detected in a particular time step (bin) is  $1/n$ . Note that the total number of straight lines (trajectories) across the sensor sensitive area  $(x, y)$  and originating from the point of the first photon detection is about  $n$ . Therefore, the probability  $P_0(n, \Delta t, M)$  for random background photons to produce a three-dimensional straight line with the total  $M$  registered photons during the time interval  $\Delta t$  in a sensor with the spatial and temporal resolution  $n$  following the detection of the first photon would be

$$P_0(n, \Delta t, M) = \frac{P_{M-1}(k_0)}{n^{M-3}}$$

During one year,  $T_Y$ , the total number of registered background photons is  $C_M T_Y \approx 3.15 \times 10^{11}$ . So, the average number  $K_0(n, \Delta t, M)$  of “false” straight lines formed by random background photons and indistinguishable from true detections of passing objects would be

$$K_0(n, \Delta t, M) = C_M T_Y P_0(n, \Delta t, M) = C_M T_Y \frac{P_{M-1}(k_0)}{n^{M-3}}$$

Let us assume a modest detector resolution,  $n = 128$ , or 7 bits. (The PSDs can have resolution up to 2048, or 11 bits, and higher.) Fig. 5 shows the number  $K_0$  of annual background-photon-produced false FOV crossing events as a function of the time interval  $\Delta t$  for the minimum required numbers of registered photons  $M$  equal to 4, 5, 6, and 7. Let us limit the number of such false events to one per year. Then, one can use the minimal numbers of

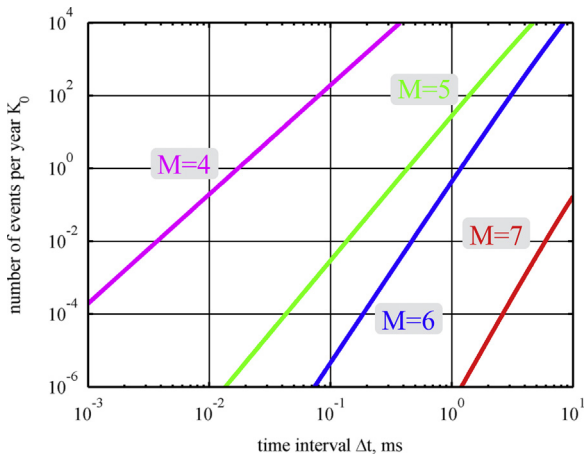


Fig. 5. Average number  $K_0$  of annual background photon random events indistinguishable from true object FOV crossings, or false debris detections, as a function of time interval  $\Delta t$  for minimum required numbers of registered photons  $M$  equal to 4 (magenta), 5 (green), 6 (blue), and 7 (red). (For interpretation of the references to color in this figure legend, the reader is referred to the web version of this article.)

registered photons  $M$  equal 4, 5, 6, and 7 for time intervals shorter than 0.017 ms, 0.432 ms, 1.19 ms, and 14.2 ms, respectively.

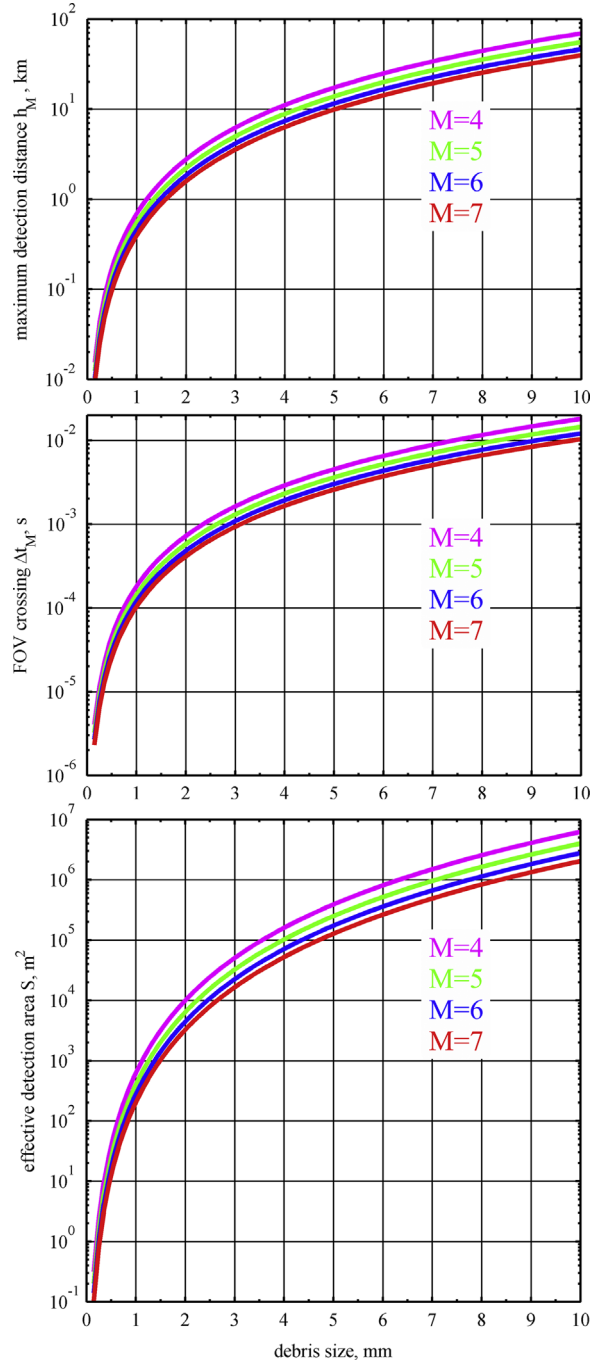


Fig. 6. Maximum detection distance  $h_M$ (top), time  $\Delta t_M$  of crossing the field of view at this maximum distance (middle), and effective detection area  $S$  (bottom) as function of the debris size (diameter) for minimum numbers of registered photons  $M$  equal 4 (magenta), 5 (green), 6 (blue), and 7 (red). All objects cross the center of the field of view with the relative velocity  $10 \text{ km s}^{-1}$  normally to the sensor axis. The maximum total sensor count rate is  $C_M = 10^4 \text{ s}^{-1}$ . (For interpretation of the references to color in this figure legend, the reader is referred to the web version of this article.)

The minimal possible number  $M$  maximizes the LODE sensitivity in identifying and extracting rare events of debris crossings. Therefore, an efficient use of the accumulated photon data would start first with considering registered photons in time intervals of 0.017 ms long and searching for events with at least 4 registered photons on straight line-trajectories in three-dimensional sensor space. Then, one considers registered photons in 0.43 ms long time intervals and search for events with at least 5 registered photons. Finally one would consider time intervals 1.2 ms and 14 ms long and search for events with 6 and 7 registered photons, respectively.

Fig. 6 illustrates sensor properties under the maximum detection distance concept: it shows dependences (Eqs. (5)–(7)) of the maximum detection distance  $h_M$  (top), the maximum time of crossing  $\Delta t_M$  the field of view at this distance, and the effective detection area  $S$  as a function of the debris size (diameter)  $a$  for the required minimum numbers of registered photons  $M$  equal 4, 5, 6, and 7. The maximum detection distance identifies the detection threshold: larger objects or objects passing closer to the sensor would produce, on average, more than the required minimal number of registered photons, resulting in detection. A passage of an object of a given size at larger distances would result in fewer than the required minimum number of registered photons and it is not detected.

Table 1 shows, as an example, the characteristics of the LODE sensor for debris with sizes 0.15, 0.3, 1, 3, and 10 mm under the maximum detection distance concept. One can see that objects 1 cm in size could be detected at distances as large as 40 km, making such observations nonlocal. On the other hand all detections of submillimeter debris would occur within 1 km from the satellite orbit. As the debris size decreases, they reflect fewer solar photons resulting in smaller maximum detection distances and effective detection areas. This decrease is somewhat compensated by a possibility to reduce the required minimum number of registered photons, as discussed above, for shorter crossing times.

Fig. 6 and Table 1 show that the LODE sensitivity (effective detection area) rapidly drops with decreasing debris size (Eq. (7)) and becomes too small for objects with sizes below 0.1 mm. Based on this dependence we can establish and consider henceforth the nominal minimal size of debris for LODE observations to be 0.2 mm.

We note here that the debris detection distance has also a minimum limit. In other words, an object passing by too close to the observer will not be detected. The minimal detection distance would reduce the effective detection area. For example, minimal distances 5 and 10 times smaller than the maximum detection distance would

result in 4% and 1% reductions of the effective detection areas, respectively.

There are two reasons for existence of the minimal detection distance. First, the field of view of a sensor mounted on a spacecraft and pointed in the antisolar direction is in the spacecraft shadow where passing by objects are not illuminated by the Sun. For example, a one meter surface would cast the umbra about 100 m long which corresponds to a maximum distance for detection of 0.4-mm debris. The shadow effect can be minimized and made negligible by pointing the sensor FOV at some angle away from the antisolar direction and mounting the sensor near the edge of the spacecraft structure rather than in the middle of the side opposite to the sun.

Second, a close passage by an object would result in a sequence of, perhaps, a couple dozen registered photons with short time intervals between them. The detector ability to register such bursts of photons would determine the minimal distance. In fact, as discussed below in Section 6, achieving the desired minimal detection distance for smallest submillimeter debris would be among most important requirements determining the specific design of the readout system of the PSD in the LODE focal plane.

Photon fluxes and their reflection by debris and detection by the PSD are random processes characterized statistically. The average number of registered photons is small and variance is relatively large. This, in turn, would result in gradual decrease of the debris detection probability with increasing distance from the observer for objects of a given size rather than in an abrupt limit of the maximum detection distance concept. Consequently, some debris would be missed when pass closer than  $h_M$  from the spacecraft as they may produce the number of registered photons smaller than  $M$ . At the same time other debris could be detected when passing at larger distances.

When an object crosses normally the FOV at a distance  $h$  it produces the mean number of registered photons  $N$  (Eq. (4)). For a random photon flux, the Poissonian distribution describes the probabilities  $p_k(N)$  to register  $k$  photons,

$$p_k(N) = \frac{N^k \exp(-N)}{k!}.$$

For the given mean number of registered photons  $N$ , one can introduce the probability  $g_M(N)$  to register at least  $M$  photons required for the reliable object detection such that

$$g_M(N) = \sum_{i=M}^{\infty} p_i(N) = 1 - \sum_{j=0}^{M-1} p_j(N).$$

**Table 1**

LODE sensor characteristics for detection of debris with sizes 0.15 mm, 0.3 mm, 1.0 mm, 3.0 mm, and 10 mm.

Size	0.15 mm	0.3 mm	1.0 mm	3.0 mm	10 mm
Required minimum number of photons	4	4	5	6	7
Max distance	15.6 m	62 m	0.55 km	4.2 km	40 km
FOV crossing time	0.0041 ms	0.016 ms	0.14 ms	1.1 ms	10 ms
Effective detection area	0.32 m <sup>2</sup>	5.1 m <sup>2</sup>	400 m <sup>2</sup>	0.023 km <sup>2</sup>	2.0 km <sup>2</sup>

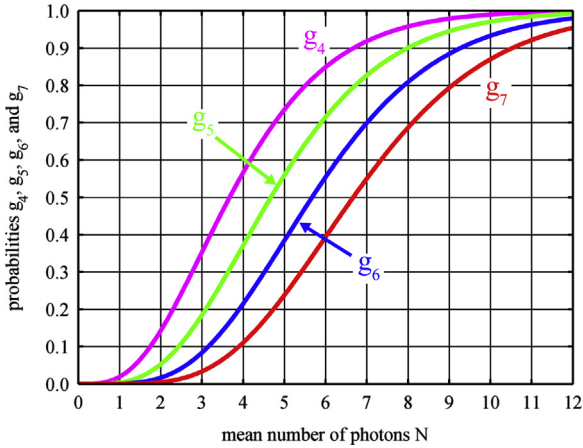


**Fig. 7.** Probabilities  $g_4$  (magenta),  $g_5$  (green),  $g_6$  (blue), and  $g_7$  (red) to register at least 4, 5, 6, and 7 photons, respectively, as a function of the mean number of registered photons  $N$ . (For interpretation of the references to color in this figure legend, the reader is referred to the web version of this article.)

Fig. 7 shows probabilities  $g_4$ ,  $g_5$ ,  $g_6$ , and  $g_7$  to register at least 4, 5, 6, and 7 photons, respectively, as a function of the mean number of the detected photons  $N$ .

Consider, for example, a 1-mm debris that produces, on average, 5 registered photons at the 0.55-km distance. This is the maximum distance for detection of such debris for  $M = 5$  (Table 1). The average number of registered photons is inversely proportional to the distance  $h$  (Eq. (4)). If such a debris crosses the FOV at the distance of 0.34 km, for example, it would produce, on average, 8 registered photons. This object passage should thus be detected under the maximum detection distance concept. In reality, because of the random nature of the photon flux and photon reflection and detection, the probability to register at least 5 photons is  $g_5(8) \approx 0.9$ . Consequently, there would be a 10% probability that fewer than the required 5 photons registered and the debris passage hence be missed. On the other hand, if such a debris crosses the FOV at the distance of 0.92 km, it would produce, on average, only 3 registered photons. Such a passage, however, would result in a probability  $g_5(3) \approx 0.2$  to register at least 5 photons and consequently this debris passage be detected with the 20% probability.

The effective debris detection area  $S_M(a)$  for a required minimum number of registered photons  $M$ , which accounts for the statistical nature of the detection, is then

$$S_M = \int_0^\infty \omega_0 h g_M dh.$$

The maximum distance concept corresponds to the function  $g_M$  equal unity at distances  $h \leq h_M$  and zero for  $h > h_M$ . Accounting for the random nature of photon fluxes and their detection would result in larger effective detection areas  $S_M$  compared to the area  $S$  obtained under the maximum distance concept for the same  $M$ . Fig. 8 shows, as an example, the dependence of the areas  $S$  and  $S_5$  for the required minimum number of registered photons  $M = 5$ . The difference between the areas decreases with increasing  $M$  and vanishes for  $M \rightarrow \infty$ .

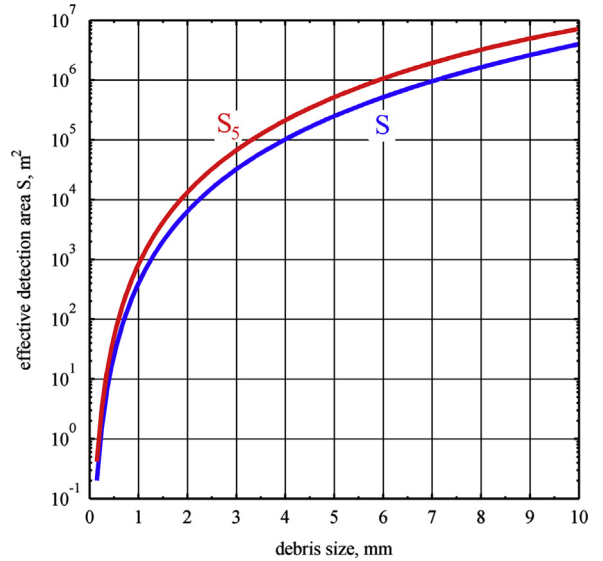


**Fig. 8.** Effective debris detection areas as a function of the debris size: the area  $S$  (blue) corresponds to the maximum detection distance concept and the area  $S_5$  (red) accounts for the statistical nature of the photon flux and its detection; the required minimum number of registered photons is  $M = 5$ . (For interpretation of the references to color in this figure legend, the reader is referred to the web version of this article.)

The minimum number of registered photons required for debris detection increases and the corresponding effective detection area decreases as time intervals of FOV crossing become larger. The time intervals correspond to certain distances from the observer and to respective minimal sizes of debris that could be detected at those distances. Therefore, one can construct a composite effective detection area  $S_0$  consisting of areas  $S_M$  for debris of certain sizes. Such an area would account for the random nature of photons but the required minimum numbers of registered photons and the corresponding sizes are determined by the simplified maximum distance concept. For the number of background-photon-produced “false” debris detections not to exceed one per year, the composite detection area  $S_0$  would be

$$S_0 = \begin{cases} S_4, & \text{for } a \leq 0.3 \text{ mm} \\ S_5, & \text{for } 0.3 \text{ mm} < a \leq 1.7 \text{ mm} \\ S_6, & \text{for } 1.7 \text{ mm} < a \leq 3.1 \text{ mm} \\ S_7, & \text{for } 3.1 \text{ mm} < a \leq 11.7 \text{ mm} \end{cases} \quad (8)$$

To estimate the number of true debris detections in one year of continuous operations, we consider a LODE sensor deployed on a spacecraft in sun-synchronous circular orbit at an 800-km altitude and inclination 98.5°. A large number of satellites operate in this region of geospace where predicted debris fluxes peak.

The NASA Handbook specifically points out that existing debris models disagree in the flux density dependence on the size, with the differences up to one order of magnitude for objects smaller than 1 cm [7]. We use here the MASTER model [53,54] which predicts fluxes lower than ORDEM [7].

For the top-level estimate purposes of this work, it is convenient to define the rate of detection  $R_0(a)$  of objects of a particular size  $a$  by simply multiplying the debris flux

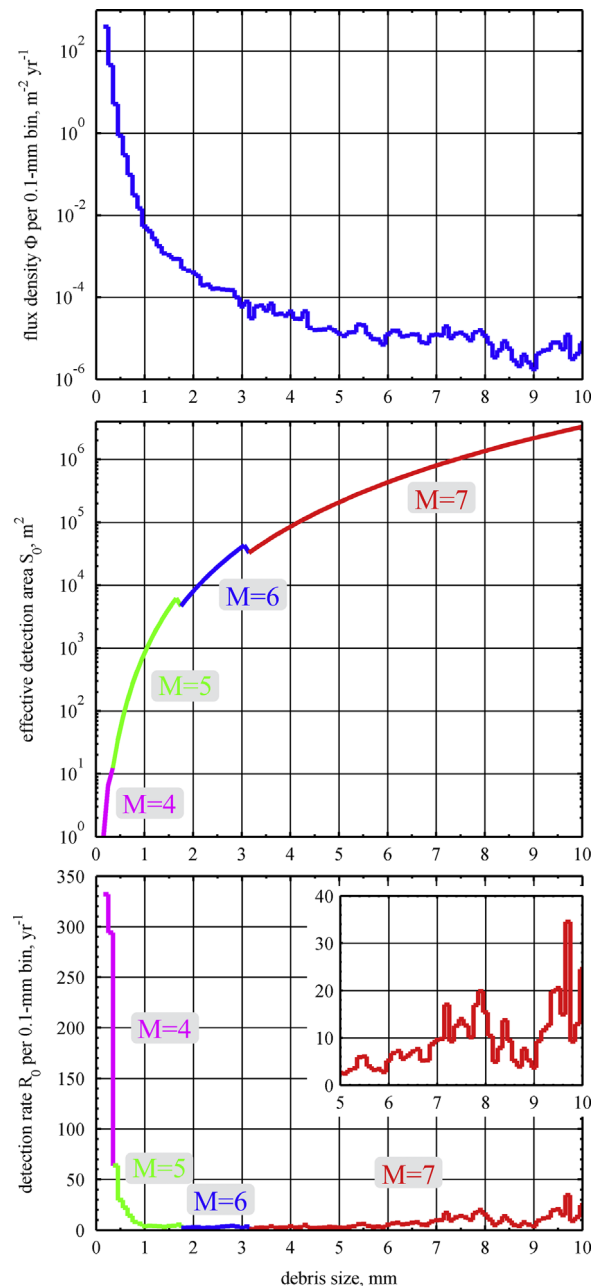


**Fig. 9.** MASTER-modeled debris flux density  $\Phi$  per 0.1-mm bin (top), composite effective detection area  $S_0$  (middle), and the annual number of debris detections (bottom) by the LODE instrument as function of the debris size (diameter) for an observer in sun-synchronous 800-km altitude circular orbit. The total number of observed 0.2–10 mm debris is about 1400 each year, including almost 780 submillimeter (0.2–1.0 mm) debris. Color coding of the curves (middle and bottom) corresponds to appropriate – for the debris size – required minimum number of registered photons 4 (magenta), 5 (green), 6 (blue), and 7 (red). The maximum total sensor count rate is  $C_M = 10^4 \text{ s}^{-1}$ . (For interpretation of the references to color in this figure legend, the reader is referred to the web version of this article.)

density  $\Phi(a)$  by the LODE effective detection area  $S_0(a)$ ,  $R_0(a) = \Phi(a)S_0(a)$ .

The rate of detection is defined, similarly to the flux density, per 0.1-mm size bins and it corresponds to the LODE sensor being pointed approximately normally to the orbital plane. Note that debris smaller than a couple millimeters are detected within a few kilometers from the observer and they are described by the local flux  $\Phi$ . Debris with a 10-mm size, for example, could be detected at distances as large as 100 km, so one would need to account for flux altitude dependence. While important, more accurate simulations of fluxes, directions, and velocities of debris should not change dramatically the rate estimates.

Fig. 9 (top) shows the model-predicted flux density of debris  $\Phi(a)$  as a function of their size per 0.1-mm bins at the selected orbit. The flux density rapidly increases with the decreasing size of debris. It is about 3 orders of magnitude larger for 1-mm debris than for 1-cm objects; the 0.2 mm debris are 4 orders of magnitude more numerous per bin than those of 1 mm in size. The middle and bottom panels of Fig. 9 show, respectively, the composite effective detection area  $S_0$  (Eq. (8)) and predicted annual numbers of detected debris as function of their size. The color-coding of the curves (middle and bottom panels) show identification of debris of different sizes by the appropriate required minimum numbers of registered photons  $M$ .

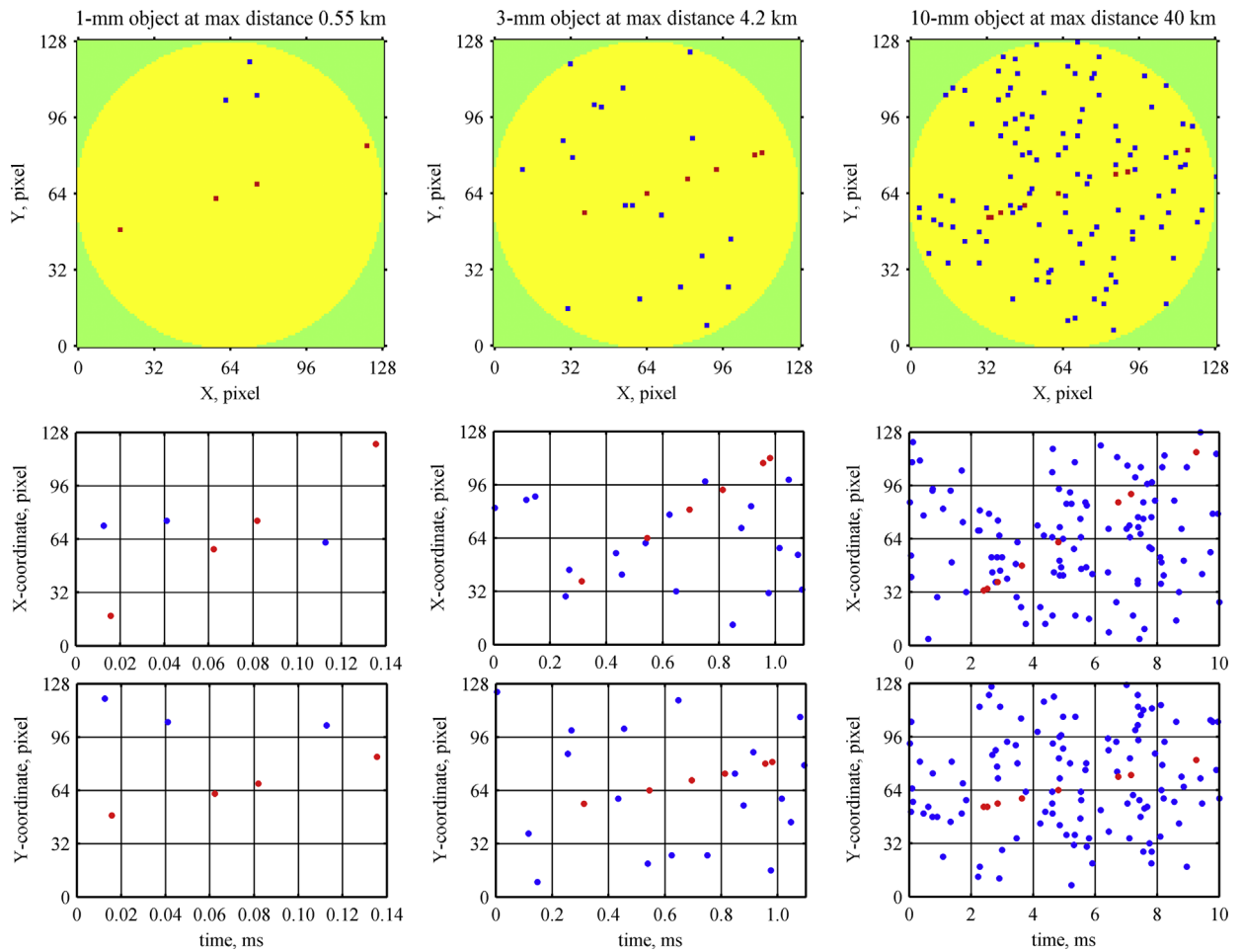
The total annual number of detected debris is about 1400, or, on average, 3.8 events per day. The annual number of object detections in the 6–10 mm size range is 465, or about 1.3 per day. Almost 780 submillimeter (0.2–1.0 mm) debris are detected annually, or 2.1 per day.

Fig. 10 illustrates LODE sensor performance by simulations of detection of debris 1, 3, and 10 mm in size crossing the FOV at corresponding maximum detection distances 0.55 km, 4.2 km, and 40 km (Table 1). The time intervals for such crossings (to be used for search of such events among photons registered in observations) are 0.14 ms, 1.1 ms, and 10 ms, respectively, and the corresponding average numbers of registered debris-reflected photons are 5, 6, and 7. The spatial resolution of the detector is  $n = 128$  pixels and the number of time steps (bins) is also 128.

Clearly, it is much easier to identify FOV crossing events for debris passing at smaller distances from the observer resulting in shorter time intervals and correspondingly smaller numbers of background photons (Fig. 10, left). During 0.1 ms, for example, there would be, on average, only one background photon detected for the adopted maximum total detector count rate limit  $C_M = 10^4 \text{ s}^{-1}$ .

## 5. Discussion and conclusions

The LODE sensor exhibits a complex response to a passing object. Since a small number of registered photons are sufficient for debris detection, the corresponding variances are relatively large. In addition, fluxes of debris and their velocities are direction dependent. Debris solar illumination as well as their albedo properties and the



**Fig. 10.** Simulated detection of the LODE FOV crossing by debris with (left-to-right) 1, 3, and 10 mm in diameter at maximum detection distances 0.55 km, 4.2 km, and 40 km, respectively, during the corresponding time intervals 0.14 ms, 1.1 ms, and 10 ms; the average numbers of registered debris-scattered photons during these time intervals are 5, 6, and 7, respectively. Top panels show two-dimensional  $128 \times 128$  pixel images accumulated during these time intervals. Red dots show debris-scattered photons while registered background photons are blue. (Dot sizes are twice as large as a pixel size in the images to improve the visibility.) The average number of background photons for given accumulation times are (left-to-right) 1.4, 11, and 100, respectively. The numbers of background and debris-reflected registered photons vary from one trial to another, as described by the Poissonian distributions, and may thus differ from the expected average numbers. The middle and bottom panels show sequences of X and Y coordinates, respectively, of registered photon as function of time. (For interpretation of the references to color in this figure legend, the reader is referred to the web version of this article.)

phase angle may also have complex dependences on observation geometry, with the sensor pointing – to avoid the spacecraft shadow – at some angle away from the antisolar direction.

A number of simplifying assumptions have been made in this work to obtain top-level estimates of expected annual numbers of the detected debris and reveal interdependencies of the sensor performance characteristics. For the latter, the concept of the maximum detection distance proved to be particularly useful.

Due to complex instrument response, a detection of a debris does not unambiguously characterize the observed object properties and trajectory. The observation of a FOV crossing would rather constrain in an important way a combination of parameters characterizing this particular object trajectory, size, albedo, and velocity. In this case, forward modeling and comparing model predictions with

observations would likely be the optimal way of science reduction of the obtained data. Forward modeling would also enable detailed trade studies of the LODE system design including specifics of the flux of targeted debris populations and their albedos, spacecraft orbit and observation geometry, and detailed sensor characteristics as well as particular approaches to data processing. Such a comprehensive study is beyond the scope of this article.

Registration of one photon by the LODE would produce approximately 100 bits of data including photon position in the focal plane and timing information as well as sensor (spacecraft) pointing. This would result in a bit rate of  $10^6$  bps for the adopted maximum total count rate  $C_M = 10^4 \text{ s}^{-1}$ . A modest spatial resolution of  $128 \times 128$  pixels seems to be sufficient for the PSD as long as its differential and integral nonlinearities do not exceed one pixel. For the LODE debris size range from 0.2–10 mm, the

corresponding detector timing accuracy, or time step  $\delta t$ , varies from  $10^{-8}$  s (10 ns) for the smallest submillimeter debris to 10  $\mu$ s for the largest. Importantly, such timing accuracies simplify time-tagging circuitry eliminating the need for special impedance-matching anodes [46,47].

From the PSD point of view, detection of smallest debris at closest (minimal) distances presents the biggest challenge. Achieving minimal detection distances that reduce effective detection areas for submillimeter debris not more than by a few per cent would require the LODE to be able to capture bursts of 10–15 registered photons within 1 microsecond with the time-tagging accuracy of 10 ns. Consequently, the PSD dead time should not exceed 50 ns. This latter requirement would play perhaps the most important role in selection of and optimizing the readout design of the focal plane position-sensitive detector. Raising the minimal size of detectable debris to 0.3 mm would significantly relax requirements to the PSD performance characteristics. The relation between the detector dead time and the minimal debris size would be an important design trade of the flight experiment.

The LODE sensor would produce large amounts of raw data,  $10^{11}$  bit per day, that could be stored on the satellite and then dumped to the ground for detailed processing. Such communication downlink bit rates are not impossible but challenging for a small satellite or a hosted payload. Real-time on-board processing will be essential to reduce the sensor bit rate transmitted to the ground. Detection of submillimeter debris requires, for example, examining time intervals shorter than 0.14 ms for search of FOV crossing events. A relatively simple real-time processing could reduce the bit rate by a factor of 100 and perhaps more. Development of more complex onboard data processing would be needed to significantly reduce the bit rate for longer time intervals. A possible efficiency of lossless data compression is difficult to estimate at this time.

The development of the focal plane PSD optimized for LODE and real-time bit rate reduction are among most challenging elements of the LODE experiment. (Many MCP detectors with different designs of readout electronics and detector high voltage power supplies are routinely flown in space physics instruments, with associated high technology readiness levels.) No special or unusual requirements to spacecraft design or mission operations have been identified. The only exception could be high-capacity of a downlink communication channel if no onboard data processing is performed. The pointing accuracy of a three-axis stabilized spacecraft could be  $0.1^\circ$  as long as better pointing knowledge is available. Note that real-time masking out of stars in the LODE data stream may also significantly reduce the required experiment bit rate. Much more precise spacecraft pointing will then be required for implementation of such an approach.

The next logical step in advancing the LODE concept is development of a comprehensive model of the entire system that takes into account realistic observational geometries of debris as predicted by MASTER/PROOF [53,54] and ORDEM [7], illumination phase angles, albedos, and statistical nature of detected photons. Such a model would establish possible accuracies of orbital parameters of

debris that could be derived from event detections and tighten the requirements to the instrument design and the MCP-based PSD and its readout system.

The performance characteristics of the narrow field of view LODE instrument are complementary to those of wide fields of view CCD-based optical sensors considered for debris detection in the past and perhaps they could be combined in a package offering unique cross-calibration and debris-characterizing capabilities. In addition, LODE optical observations would complement those by the Haystack and HAX radar which may open an important opportunities for better characterizing responses of both optical sensors and radar in detecting small debris.

A LODE sensor in LEO will likely obtain enough statistically significant data to contribute to constraining debris models after one year of observations. Continuing multi-year operations of the instrument may also be able to reveal temporal variations in debris fluxes and perhaps even discover fragmentation events. Deploying LODE sensors on spacecraft beyond LEO, for example in geostationary transfer orbit, could also observe small debris in geostationary orbit and micrometeoroids fluxes. In addition, the LODE sensor may be able to characterize possible dust fluxes in lunar environment if deployed on a Moon-orbiting spacecraft or lunar surface.

To conclude, the performance characteristics of the LODE experimental and instrumental concept show that submillimeter and millimeter debris could be measured by a passive optical sensor based on a photon-counting time-tagging imager. Such observation would complement those obtained by optical telescopes and radar and could significantly reduce uncertainties and constrain debris models, thus directly contributing to optimum design and safe operations of space systems and to mission safety and assurance.

## References

- [1] D.J. Kessler, B.G. Cour-Palais, Collision frequency of artificial satellites: the creation of a debris belt, *J. Geophys. Res.* 83 (1978) 2646–2673, <http://dx.doi.org/10.1029/JA083iA06p02637>.
- [2] N.L. Johnson, D.S. McKnight, *Artificial Space Debris*, Krieger Publ. Co., Malabar, FL, 1991.
- [3] National Research Council, *Orbital Debris: A Technical Assessment*, National Academy Press, Washington, DC, 1995.
- [4] N.N. Smirnov (Ed.), *Space Debris: Hazard Evaluation and Mitigation*, Taylor and Francis, London, 2002.
- [5] H. Klinkrad, *Space Debris: Models and Risk Analysis*, Springer-Praxis, 2006.
- [6] J.-C. Liou, N.L. Johnson, Risks in space from orbiting debris, *Science* 311 (2006) 340–341, <http://dx.doi.org/10.1126/science.1121337>.
- [7] NASA-Handbook 8719.14, Handbook for limiting orbital debris, NASA, Washington, DC, 2008.
- [8] N.L. Johnson, U.S. space surveillance, *Adv. Space Res.* 13 (8) (1993) (8)5–(8)20, [http://dx.doi.org/10.1016/0273-1177\(93\)90563-Q](http://dx.doi.org/10.1016/0273-1177(93)90563-Q).
- [9] V. Dicky, Z. Khutorovsky, A. Kuricshah, A. Menshikov, R. Nazirov, A. Pitsyck, S. Veniaminov, V. Yurasov, The Russian space surveillance system and some aspects of spaceflight safety, *Adv. Space Res.* 13 (8) (1993) 21–31, [http://dx.doi.org/10.1016/0273-1177\(93\)90564-R](http://dx.doi.org/10.1016/0273-1177(93)90564-R).
- [10] Factsheet, USSTRATCOM Space Control and Space Surveillance, ([http://www.stratcom.mil/factsheets/USSTRATCOM\\_Space\\_Control\\_and\\_Space\\_Surveillance/printable/](http://www.stratcom.mil/factsheets/USSTRATCOM_Space_Control_and_Space_Surveillance/printable/)); (accessed 23.12.2013).
- [11] N.L. Johnson, E. Stansbery, J.-C. Liou, M. Horstman, C. Stokely, D. Whitlock, The characteristics and consequences of the break-up of the Fengyun-1C spacecraft, *Acta Astronaut.* 63 (2008) 128–135, <http://dx.doi.org/10.1016/j.actaastro.2007.12.044>.

- [12] Fengyun-1C Debris: one year later, *Orbital Debris Quarterly Newsletter*, 12(1) (2008) 2–3.
- [13] H. Krag, M. Kahl, J. Bendisch, H. Klinkrad, and T. Schildknecht, Space based optical observation of small debris objects, in: *Proceedings of the Third European Conference on Space Debris*, ESA SP-473, Vol. 1, pp. 147–152, ESA Publ. Div., Noordwijk, The Netherlands, 2001.
- [14] T. Flohrer, H. Krag, H. Klinkrad, T. Schildknecht, Feasibility of performing space surveillance tasks with a proposed space-based optical architecture, *Adv. Space Res.* 47 (2011) 1029–1042, <http://dx.doi.org/10.1016/j.asr.2010.11.021>.
- [15] E. Knott, Radar cross sections, in: M.I. Skolnik (Ed.), *Radar Handbook*, 2nd edition, McGraw-Hill, Boston, Mass., 1990, pp. 11.1–11.56.
- [16] J.W. Waters, Absorption and emission of atmospheric gases, *Astrophysics*, Part B: Radio Telescopes (Series: Methods of experimental physics, V. 12), Academic Press, New York, 1976, 142–176 (Chapter 2.3).
- [17] E.G. Stansbery, G. Bohannon, C. Pitts, T. Tracy, J. Stanley, Radar observations of small space debris, *Adv. Space Res.* 13 (8) (1993) 43–48, [http://dx.doi.org/10.1016/0273-1177\(93\)90566-T](http://dx.doi.org/10.1016/0273-1177(93)90566-T).
- [18] J. Hamilton, NASA develops report on radar observations of small debris populations, *Orbital Debris Quarterly Newsletter* 17 (4) (2013) 4–5.
- [19] D.C. Harrison, J.C. Chow, The space-based visible sensor, *Johns Hopkins APL Techn. Digest* 17 (2) (1996) 226–236.
- [20] E.M. Gaposchkin, C. von Braun, J. Sharma, J. Guidance, *Control, Dyn.* 23 (2000) 148–152, <http://dx.doi.org/10.2514/2.4502>.
- [21] D.R. Lobb, J.S.B. Dick, S.F. Green, Development of concepts for detection and characterization of debris in Earth orbit using passive optical instruments, *Adv. Space Res.* 13 (8) (1993) 59–63, [http://dx.doi.org/10.1016/0273-1177\(93\)90568-V](http://dx.doi.org/10.1016/0273-1177(93)90568-V).
- [22] T. Flohrer, J. Peitonen, A. Kramer, T. Eronen, J. Kuusela, E. Riihonen, T. Schildknecht, E. Stoveken, E. Valtonen, F. Wokke, and W. Flury, Space-based optical observations of space debris, In: *Proceedings of the Fourth European Conference on Space Debris*, Darmstadt, Germany, ESA SP-587, 2005.
- [23] W. Priedhorsky, J.J. Bloch, Optical detection of rapidly moving objects in space, *Appl. Opt.* 44 (2005) 423–432, <http://dx.doi.org/10.1364/AO.44.000423>.
- [24] M. Oswald, H. Krag, P. Wegener, B. Bischof, Concept for an orbital telescope observing the debris environment in GEO, *Adv. Space Res.* 34 (2004) 1155–1159, <http://dx.doi.org/10.1016/j.asr.2003.01.022>.
- [25] J.R. Shell, Optimizing orbital debris monitoring with optical telescopes, In: *Proceedings of the Advanced Maui Optical and Space Surveillance Technologies Conference*, p. E42, ed: S. Ryan, Wailea, Maui, Hawaii, September 14–17, 2010.
- [26] G.D. Arndt, P. Fink, W.B. Warren, A space station-based orbital debris-tracking system, *Adv. Space Res.* 13 (8) (1993) 65–68, [http://dx.doi.org/10.1016/0273-1177\(93\)90569-W](http://dx.doi.org/10.1016/0273-1177(93)90569-W).
- [27] C. Firmani, L. Gutierrez, E. Ruiz, G.F. Bisiacchi, L. Salas, F. Paresce, Astronomical applications of the MEPSICRON photon detector, *Proc. SPIE 0445 (Instrumentation in Astronomy V)* (1984) 192–198, <http://dx.doi.org/10.1117/12.966148>.
- [28] J. Barnstedt, M. Gutekunst, M. Grewing, L. Bianchi, Astronomical test of a photon-counting detector, *Mitteilungen der Astronomischen Gesellschaft* 62 (1984) 356–359.
- [29] B.E. Woodgate, R.A. Kimble, C.W. Bowers, S. Kraemer, M.E. Kaiser, A.C. Danks, J.F. Grady, J.J. Loiacono, M. Brumfield, L. Feinberg, T.R. Gull, S.R. Heap, S.P. Maran, D. Lindler, D. Hood, W. Meyer, C. VanHouten, V. Argabright, S. Franka, R. Bybee, D. Dorn, M. Bottema, R. Woodruff, D. Michika, J. Sullivan, J. Hetlinger, C. Ludtke, R. Stocker, A. Delamere, D. Rose, I. Becker, H. Garner, J.G. Timothy, M. Blouke, C.L. Joseph, G. Hartig, R.F. Green, E.B. Jenkins, J.L. Linsky, J.B. Hutchings, H.W. Moos, A. Boggess, F. Roesler, D. Weistrop, The space telescope imaging spectrograph design, *Publ. Astron. Soc. Pacif.* 110 (1998) 1183–1204, <http://dx.doi.org/10.1086/316243>.
- [30] J.C. Green, C.S. Froning, S. Osterman, D. Ebbets, S.H. Heap, C. Leitherer, J.L. Linsky, B.D. Savage, K. Sembach, J.M. Shull, O.H.W. Siegmund, T.P. Snow, J. Spencer, S.A. Stern, J. Stocke, B. Welsh, S. Béland, E.B. Burgh, C. Danforth, K. France, B. Keeney, J. McPhate, S.V. Penton, J. Andrews, K. Brownsberger, J. Morse, E. Wilkinson, The cosmic origins spectrograph, *Astrophys. J.* 744 (2012) 60, <http://dx.doi.org/10.1088/0004-637X/744/1/60>.
- [31] C. Ho, W. Priedhorsky, M. Baron, Detecting small debris using a ground-based photon counting detector, *Proc. SPIE 1951 (1993)* 67–75, <http://dx.doi.org/10.1117/12.156561>.
- [32] M.C. Roggemann, K. Hamada, S.R. Gudimetla, K. Luu, L.W. Bradford, D.C. Thompson and R. Shirey, Remote Ultra-Low Light Imaging (RULLI) for Space Situational Awareness (SSA): modeling and simulation results for passive and active SSA, *Proc. SPIE 7094 (Unconventional Imaging IV)*, eds. J.J. Dolne, T.J. Karr, and V.L. Ganitz, 2008, 709409, <http://dx.doi.org/10.1117/12.793913>.
- [33] M. Lampton, Microchannel plates and their applications to photon counting image systems, *Proc. IAU Colloq.* 40, ed. M. Duchesne and G. Lelievre, Observatoire de Paris-Meudon, France, pp. 32/1–32/28, 1977.
- [34] J.G. Timothy, Optical detectors for spectroscopy, *Publ. Astron. Soc. Pacif.* 95 (1983) 810–834, <http://dx.doi.org/10.1086/131258>.
- [35] M. Gruntman, Coordinate-sensitive detectors based on multichannel plates (review), *Instrum. Experim. Techn.* 27 (1) (1984) 1–19.
- [36] G.W. Fraser, *X-ray Detectors in Astronomy*, Cambridge Univ. Press, Cambridge, 1989.
- [37] C.L. Joseph, Advances in astronomical UV image sensors and associated technologies, *Proc. SPIE*, 2999 (1997) 244–258, <http://dx.doi.org/10.1117/12.271197>.
- [38] J.V. Vallergera, B.Y. Welsh, O.H.W. Siegmund, The future of imaging photon counting detectors for ground-based astronomy, *Proc. SPIE 4841 (2003)* 795–804, <http://dx.doi.org/10.1117/12.461098>.
- [39] O.H.W. Siegmund, J.V. Vallergera, A.S. Tremsin, J. McPhate, X. Michalet, R.A. Colyer and S. Weiss, Microchannel plate imaging photon counters for ultraviolet through NIR detection with high time resolution, *Proc. SPIE 8033 (Advanced Photon Counting Techniques V)*, 2011, <http://dx.doi.org/10.1117/12.884271>.
- [40] M.R. Ainbund, L.S. Gorn, M.A. Gruntman, D.S. Zakharov, A.A. Klimashev, V.B. Leonas, I.P. Maslennikov, B.I. Khazanov, Coordinate-sensitive detector on the basis of microchannel plates, *Instrum. Experim. Techn.* 27 (1) (1984) 68–73.
- [41] O.H.W. Siegmund, M. Lampton, J. Bixier, S. Chakrabarti, J. Vallergera, S. Bowyer, R.F. Malina, Wedge and strip image readout systems for photon-counting detectors in space astronomy, *J. Opt. Soc. Am. A* 3 (1986) 2139–2145, <http://dx.doi.org/10.1364/JOSAA.3.002139>.
- [42] M. Lampton, O. Siegmund, R. Raffanti, Delay line anodes for microchannel plate spectrometers, *Rev. Sci. Instrum.* 58 (1987) 2298–2305, <http://dx.doi.org/10.1063/1.1139341>.
- [43] J.G. Timothy, J.S. Morgan, D.C. Slater, D.B. Kastle, R.L. Bybee, H.E. Culver, MAMA detector systems: a status report, *Proc. SPIE 1158 (Ultraviolet Technology III)* (1989) 104–117, <http://dx.doi.org/10.1117/12.962535>.
- [44] O.H.W. Siegmund, M.A. Gummin, J.M. Stock, D.R. Marsh, R. Raffanti, J.S. Hull, High-resolution monolithic delay-line readout techniques for two-dimensional microchannel plate detectors, *Proc. SPIE 2006 (EUV, X-Ray, and Gamma-Ray Instrumentation for Astronomy IV)*, (1993) 176–187, <http://dx.doi.org/10.1117/12.162851>.
- [45] J.V. Vallergera, J.B. McPhate, A.P. Martin, G.A. Gaines, O.H.W. Siegmund, E. Wilkinson, S. Penton, S. Beland, The HST-COS far-ultraviolet detector: final ground calibration, *Proc. SPIE 4498 (UV/EUV and Visible Space Instrumentation for Astronomy and Solar Physics)* (2001) 141–151, <http://dx.doi.org/10.1117/12.450052>.
- [46] J.L. Wiza, Microchannel plate detectors, *Nucl. Instrum., Meth.* 162 (1979) 587–601.
- [47] M. Gruntman, Energetic neutral atom imaging of space plasmas, *Rev. Sci. Instrum.* 68 (1997) 3617–3656, <http://dx.doi.org/10.1063/1.1148389>.
- [48] Ch. Leinert, S. Bowyer, L.K. Haikala, M.S. Hanner, M.G. Hauser, A.-Ch. Levasseur-Regourd, I. Mann, K. Mattila, W.T. Reach, W. Schlosser, H.J. Staude, G.N. Toller, J.L. Weiland, J.L. Weinberg, A.N. Witt, The 1997 reference of diffuse night sky brightness, *Astron. Astrophys.* 127 (1998) 1–9, <http://dx.doi.org/10.1051/aas:1998105>. (Suppl. Ser.).
- [49] G.N. Toller, Optical observations of galactic and extragalactic light: implications for galactic structure (*Proc. 139th IAU Symp.*), in: S. Bowyer, G. Leinert (Eds.), *The Galactic and Extragalactic Background Radiation*, Kluwer Academic Publ., Dordrecht, [http://dx.doi.org/10.1007/978-94-009-0653-2\\_2](http://dx.doi.org/10.1007/978-94-009-0653-2_2).
- [50] O. Siegmund, J. Vallergera, B. Welsh, J. McPhate, and A. Tremsin, High speed optical imaging photon counting microchannel plate detectors for astronomical and space sensing applications, In: *Proceedings of*

- the Advanced Maui Optical and Space Surveillance Technologies Conference, ed: S. Ryan, Wailea, Maui, Hawaii, September 1–4, 2009.
- [51] A. Hirshfeld, R.W. Sinnott, F. Ochsenbein, 2nd edition, *Sky Catalogue 2000.0, Vol. 1*, Cambridge University Press, New York, NY, 1991.
- [52] M. Mulrooney, M. Matney, M. Hejduk, and E. Barker, An investigation of global albedo values, In Proceedings of the Advanced Maui Optical and Space Surveillance Technologies Conference, p. E65, ed.: S. Ryan, Maui, Hawaii, 2008.
- [53] J. Bendisch, K. Bunte, H. Klinkrad, H. Krag, C. Martin, H. Sdunnus, R. Walker, P. Wegener, C. Wiedemann, The MASTER-2001 model, *Adv. Space Res.* 34 (2004) 959–968, <http://dx.doi.org/10.1016/j.asr.2003.02.026>.
- [54] C. Wiedemann, S. Flegel, J. Gelhaus, M. Moeckel, H. Klinkrad, H. Krag, and P. Voersmann, The space debris environment model MASTER-2009, In: Proceedings of the 28th International Symposium Space Technical Science (ISTS), Okinawa, Japan, 2011.



**Mike Gruntman** is Professor of Astronautics at the University of Southern California (USC); he is the founder of the USC Astronautics Program and served the founding chairman of the Department of Astronautical Engineering from 2004–2007. His research interests include astronautics, space physics, instrumentation and sensors, rocketry and propulsion, satellite design and technologies, space debris, space education, and history of rocketry and spacecraft. Mike authored and co-authored 270 publications, including 85+ journal articles and book chapters and 3 books. He received IAA's Luigi Napolitano Book Award in 2006. Dr. Gruntman is Corresponding Member of IAA and Associate Fellow of AIAA.